Journal of the Air & Waste Management Association
Publication details, including instructions for authors and subscription information:
http://www.tandfonline.com/loi/uawm20

A Model to Predict the System Performance of an Electrostatic Precipitator for Collecting Polydisperse Particles

Hsunling Bai [a] , Chungsying Lu [b] & Chung Liang Chang [a]
[a] Institute of Environmental Engineering, National Chiao-Tung University , Hsin-Chu , Taiwan
[b] Department of Environmental Engineering , National Chung Hsing University , Taichung , Taiwan
Published online: 05 Mar 2012.

To cite this article: Hsunling Bai , Chungsying Lu & Chung Liang Chang (1995) A Model to Predict the System Performance of an Electrostatic Precipitator for Collecting Polydisperse Particles, Journal of the Air & Waste Management Association, 45:11, 908-916, DOI: 10.1080/10473289.1995.10467423

To link to this article: http://dx.doi.org/10.1080/10473289.1995.10467423

TECHNICAL PAPER

ISSN 1047-3289 *J. Air & Waste Manage. Assoc.* **45**: 908-916

A Model to Predict the System Performance of an Electrostatic Precipitator for Collecting Polydisperse Particles

Hsunling Bai
Institute of Environmental Engineering, National Chiao-Tung University, Hsin-Chu, Taiwan

Chungsying Lu
Department of Environmental Engineering, National Chung Hsing University, Taichung, Taiwan

Chung Liang Chang
Institute of Environmental Engineering, National Chiao-Tung University, Hsin-Chu, Taiwan

ABSTRACT

This paper presents a model for predicting the performance of an electrostatic precipitator (ESP) for collecting polydisperse particles. The particle charge was obtained by modifying Cochet's charge equation; the particle size distribution was approximated by a lognormal function; and then the statistic method of moments was employed to obtain a set of the first three moment equations. The continuous evolution of the particle size distribution in an ESP is easily taken into account by the first three moment equations. The performance of this model was validated by comparing its predictions with the existing data available in the literature. Effects of the particle size distribution on the ESP performance were examined, and the results indicated that both overall mass and number efficiencies are lower for inlet particles with a larger mass median diameter and a higher geometric standard deviation. The methodology introduced may be applied to develop design criteria and determine optimal operating conditions of an ESP for improving the collection efficiency of the submicron particles.

INTRODUCTION

Electrostatic precipitators (ESPs) are one of the most common particulate control devices used to control fly ash emissions from utility boilers, incinerators, and many industrial processes. The first mathematic model of ESP performance is the famous Deutsch-Anderson equation,[1]

$$\eta = 1 - \exp\left(-\frac{A_c V_e}{Q}\right) \tag{1}$$

where η is the collection efficiency, A_c is the collector surface area, V_e is the effective migration velocity of particles, and Q is the volumetric flow rate of gas through the unit. Although the Deutsch-Anderson equation is widely used in the design of ESPs, its assumptions of monodisperse particles and constant effective migration velocity of particles in the ESP restrict its ability to provide accurate predictions.

A common industrial application of the Deutsch-Anderson equation is to compute the grade efficiency over all particle size spectrum, and then integrate the grade efficiency for obtaining the overall mass efficiency as given by[2]

$$\eta_m = \frac{\int_0^\infty \eta(d_p) d_p^3 n_i(d_p) d(d_p)}{\int_0^\infty d_p^3 n_i(d_p) d(d_p)} \tag{2}$$

where $\eta(d_p)$ is the grade efficiency, d_p is the particle diameter, and $n_i(d_p)$ is the inlet particle size distribution function. Feldman[3] employed this approach and modified the Deutsch-Anderson equation by assuming a lognormal size distribution function. The grade efficiency appearing in his model is

$$\eta(d_p) = 1 - \exp\left\{\frac{A_c \varepsilon_0 E_{av}^2 C d_p}{3\mu Q}\left[\left(1+\frac{2\lambda}{d_p}\right)^2 + \frac{2(\kappa-1)}{\left(1+\frac{2\lambda}{d_p}\right)(\kappa+2)}\right]\right\} \tag{3}$$

where ε_0 is the permittivity of free space, E_{av} is the average field strength, C is the Cunningham slip correction factor, μ is the fluid viscosity, λ is the mean free path of the gas, and κ is the dielectric constant of the particle.

Gooch and Francis[4] also incorporated a lognormal size distribution function in their ESP model and reported that both the mass median diameter (MMD) and the geometric standard deviation (σ_g) have profound effects on the overall mass

IMPLICATIONS

Since the passage of the Clean Air Act Amendments of 1990 in the United States, toxic substances in fine fly ash particles have been of concern around the world. The overall mass efficiency traditionally used for a particulate control device is insufficient to clearly confirm that toxic substances collect on the fly ash particles. This paper presents a model to predict the overall mass and number efficiencies of an ESP. By applying this model, the operation and design of an ESP can be improved, and the collection efficiency of submicron particles (and therefore the toxic substances in fine fly ash particles) can be increased.

efficiency. The overall mass efficiency increases with increasing MMD or decreasing σ_g. Recently a study of the effect of the particle size distribution on the effective migration velocity of particles was conducted by Riehle and Löffler.[5] In their study, a lognormal inlet particle size distribution was assumed and they concluded that σ_g has a significant influence on the effective migration velocity of particles in the ESP.

Although the polydisperse nature of particles can be accounted for by the integration of grade efficiency, it usually requires one to be familiar with numerical analysis, such as the Gauss-Hermite quadrature method.[2] In addition, when more complicated mechanisms (such as fluid dynamics and the space charge effect, which may influence the particle transport behavior) are to be incorporated into the model, the integration method often requires a significant computational effort.

Another widely employed ESP model accounting for the polydisperse nature of particles is the Matts-Ohnfeldt Model,[6]

$$\eta = 1 - \exp\left(-\frac{A_c V_{ek}}{Q}\right)^k \qquad (4)$$

where k is an adjustable parameter which normally ranges from 0.4 to 0.6. Since this method employs a rough estimate of particle polydispersity, it is simpler than the integration method used by Feldman[3] and Gooch and Francis.[4]

Although the above models account for the effects of particle polydispersity, the continuous change of the particle size distribution along the ESP may not be easily considered. Furthermore, most ESP models predict the mass efficiency, with which the collection of submicron particles could not be actually evaluated. And it is known that concentrations of many toxic substances are higher in fine fly ash particles than in coarse particles.[7] Therefore the collection efficiency, in terms of the particle number, would be more meaningful for the collection of submicron particles.

The goal of this study is to present a model considering the continuous evolution of lognormally distributed particles in terms of the moments over the entire particle size spectrum for predicting the overall mass and number efficiencies of an ESP. The performance of this model is validated by comparing its predictions with the existing data available in the literature. Effects of the specific collecting area (SCA) and the particle size distribution on the overall mass and number efficiencies of an ESP are investigated and quantitatively determined.

MODEL DEVELOPMENT

Basic Assumptions

The following major assumptions are made in developing the proposed model to study the performance of an ESP :

1. The system is in a steady-state operating condition.
2. Particle resistivity is not considered in this model.
3. Effects of gas leakage and rapping reentrainment are neglected.
4. An average dust flow velocity is used which approximates the actual velocity profile.
5. The size distribution is approximated by a lognormal function throughout the ESP.
6. The particle saturation charge is attained in a very short time, compared to the total residence time of particles.

Mass Balance Equation

The schematic diagram of a dust stream flowing through a plate-plate or wire-plate ESP is shown in Figure 1. The mass balance equation in terms of the particle size distribution function, n(v), over a control volume of finite length, Δx, is given by

$$A_p U_{av}(n(v)|_x - n(v)|_{x+\Delta x}) = V_e A_c n(v)|_x \qquad (5)$$

where A_p is the precipitator cross sectional area (= h w); h is the height of the collecting plate; w is the space between two parallel plates; U_{av} is the average dust flow velocity; v is the particle volume; and x is the axial distance. The collector surface area (A_c) is equal to $2h\Delta x$. The left-hand term of equation (5) accounts for the flow convection, while the right-hand term accounts for the external electrostatic force. On dividing both sides by Δx and taking the limit as Δx goes to zero, equation (5) becomes

$$U_{av}\frac{d\,n(v)}{dx} = -2\frac{V_e\,n(v)}{w} \qquad (6)$$

Once the effective migration velocity of particles is determined, the evolution of the particle size distribution function, n(v), along an ESP can be solved using equation (6). The effective migration velocity of a particle of diameter d_p is[8]

$$V_e = \frac{q\,E_c\,C}{3\pi\mu d_p} \qquad (7)$$

where q is the particle charge and E_c is the electric field strength at the collector surface.

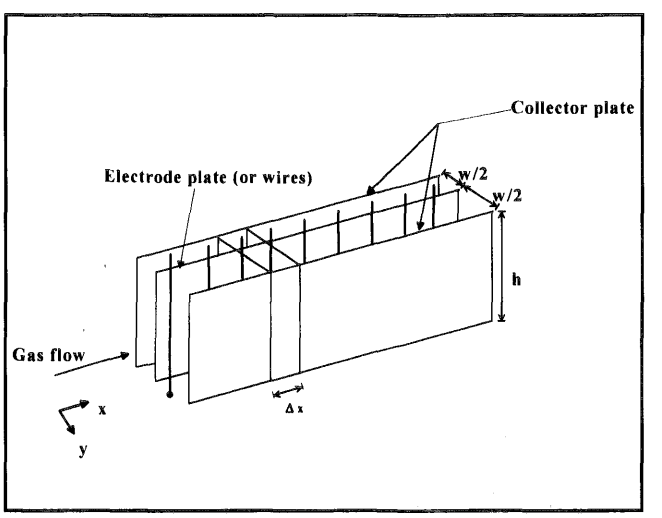

Figure 1. Schematic diagram of a dust stream flowing through a plate-plate or wire-plate electrostatic precipitator.

Particle Charge Equation

The particle charge (q) is a function of particle size, and can be described by Cochet's charge equation[9]

$$q = [(1+\frac{2\lambda_i}{d_p})^2 + \frac{2}{1+\frac{2\lambda_i}{d_p}}\frac{\kappa-1}{\kappa+2}]\,\pi\,\varepsilon_0 E_\infty d_p^2 \qquad (8)$$

where λ_i is the ionic mean free path and E_∞ is the local electric field strength. Although Cochet's equation is simple compared to other particle charge theories, it is not an integrable form. Therefore Cochet's equation is brought into an integrable form by the following procedures.

Fine particle charge. For fine particles much smaller than the ionic mean free path ($\lambda_i/d_p \gg 1$), the second term in the bracket of equation (8) can be ignored. The particle charge equation is thus simplified as

$$q_f = (1+\frac{2\lambda_i}{d_p})^2\,\pi\varepsilon_0 E_\infty d_p^2 \qquad (9)$$

A further simplification can be made by approximating $(1+2\lambda_i/d_p)^2$ to $(2\lambda_i/d_p)$,[2] given by

$$q_f = 4\pi\lambda_i^2\varepsilon_0 E_\infty \qquad (10)$$

Coarse particle charge. For coarse particles much larger than the ionic mean free path ($\lambda_i/d_p \gg 1$), the value of $2\lambda_i/d_p$ for the first and second terms in the bracket of equation (8) can be neglected. The particle charge equation is thus simplified as

$$q_c = (1+2\frac{\kappa-1}{\kappa-2})\,\pi\varepsilon_0 E_\infty d^2_p \qquad (11)$$

Total particle charge. Both equations (10) and (11) have maximum departures from Cochet's equation as values of $2\lambda_i/d_p$ approach unity. However, departures are found to be minimum if these two equations are additive. Hence the particle charge in terms of particle volume (v) over the entire particle size spectrum is a combination of the two equations and is expressed as

$$q = q_1 + q_2 v^{\frac{2}{3}} \qquad (12)$$

where

$$q_1 = q_f = 4\pi\lambda_i^2\varepsilon_0 E_\infty \qquad (13)$$

and

$$q_2 = q_c/v^{\frac{2}{3}} = (1+2\frac{\kappa-1}{\kappa+2})\pi\varepsilon_0 E_\infty (\frac{6}{\pi})^{\frac{2}{3}} \qquad (14)$$

A comparison of the particle charges using the modified form of Cochet's equation and the original form of Cochet's equation is shown in Figure 2. The approximation is quite close to the charges predicted by Cochet's equation, with some differences for fine particles. The agreement would be better if equation (9) was used instead for fine particle charge. However, equation (10) is employed in the following study for computational simplicity.

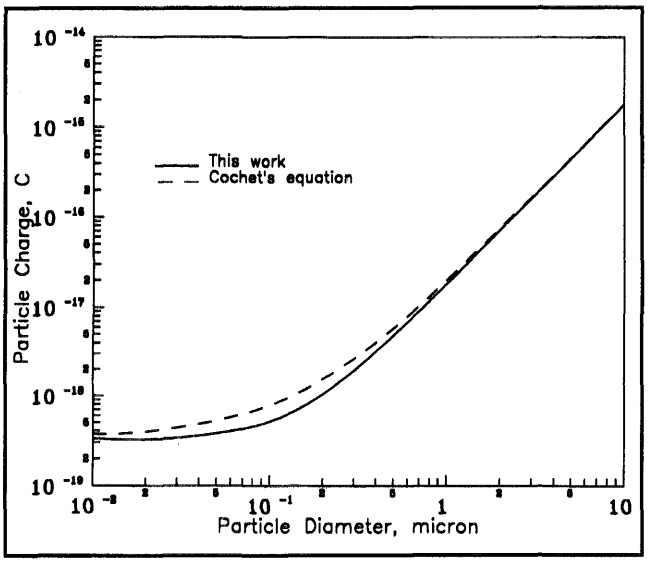

Figure 2. The particle charges predicted by the modified Cochet's equation and by Cochet's equation.

Cunningham slip correction factor. Similarly, the Cunningham slip correction factor can also be brought into an integrable form by using the approximation proposed by Bai and Biswas:[10]

$$c = C^* + 3.314\frac{\lambda}{d_p} \qquad (15)$$

where $C^* = 0.56$ for $\lambda/d_p > 1$ and $C^* = 1$ for $\lambda/d_p \leq 1$.

Effective migration velocity. The electric field strength at the collector surface (E_c) and the local electric field strength (E_∞) can be assumed to equal the average field strength (E_{av}) in a single-stage ESP.[2] Substituting equations (12) and (15) into equation (7), the effective migration velocity of a particle is written as

$$v_e = (q_1 q_4 v^{-\frac{2}{3}} + q_1 q_3 v^{-\frac{1}{3}} + q_2 q_4 + q_2 q_3 v^{\frac{1}{3}}) \qquad (16)$$

where

$$q_3 = \frac{E_{av} C^*}{3\pi\mu}(\frac{\pi}{6})^{\frac{1}{3}} \qquad (17)$$

and

$$q_4 = \frac{3.314\lambda\, E_{av}}{3\pi\mu}(\frac{\pi}{6})^{\frac{2}{3}} \qquad (18)$$

Method of moments. The use of moments has the advantage of simplicity in evaluating the continuous evolution of polydisperse particles. However, a close set of moment equations can not be obtained unless the shape of the size distribution is represented by a specific function. For this

purpose, a lognormal function is used, since most ESP models characterize the particle size distribution by a lognormal function. The jth moment of a particle size distribution is[11]

$$M_j = \int_0^\infty v^j n(v)\, dv \tag{19}$$

while the size distribution function, n(v), for lognormally distributed particles is defined as[8]

$$n(v) = \frac{N}{3\sqrt{2\pi}\ln\sigma_g} \exp\left[-\frac{\ln_2(v/v_g)}{18\ln^2\sigma_g}\right]\frac{1}{v} \tag{20}$$

where N is the total particle number concentration, v_g is the geometric mean particle volume, and σ_g is the geometric standard deviation. Values of v_g and σ_g can be expressed in terms of the first three moments of the distribution as[12]

$$v_g = \frac{M_1^2}{M_0^{3/2}M_2^{1/2}} \tag{21}$$

$$\ln^2\sigma_g = \frac{1}{9}\ln\left(\frac{M_0M_2}{M_1^2}\right) \tag{22}$$

where M_0 is the zeroth moment which represents the total particle number concentration (= N); M_1 is the first volume moment which denotes the total particle volume; M_2 is the second volume moment which indicates the amount of light scattered due to the particles' exit from the ESP. Thus, the first three moments of the distribution are sufficient to describe the behavior of the size distribution of lognormally preserving particles and the jth moment of the distribution can be written in terms of M_0, v_g, and σ_g as[12]

$$M_j = M_0 v_g^j \exp(4.5\, j^2 \ln^2\sigma_g) \tag{23}$$

Model equations. Substituting equation (16) into equation (6), multiplying both sides by $v^j\, dv$, and integrating over the entire particle size spectrum, the continuous evolution of the first three moments of the distribution along the ESP are given by

$$U_{av}\frac{dM_0}{dx} = -\frac{2}{w}V_{e0}M_0 \tag{24}$$

$$U_{av}\frac{dM_1}{dx} = -\frac{2}{w}V_{e1}M_1 \tag{25}$$

$$U_{av}\frac{dM_2}{dx} = -\frac{2}{w}V_{e2}M_2 \tag{26}$$

and

$$v_{e0} = q_1q_4v_g^{-\frac{2}{3}}\exp(2\ln^2\sigma_g) + q_1q_3v_g^{-\frac{1}{3}}\exp(0.5\ln^2\sigma_g) + q_2q_4 + q_2q_3v_g^{\frac{1}{3}}\exp(0.5\ln^2\sigma_g) \tag{27}$$

$$v_{e1} = q_1q_4v_g^{-\frac{2}{3}}\exp(-4\ln^2\sigma_g) + q_1q_3v_g^{-\frac{1}{3}}\exp(-2.5\ln^2\sigma_g) + q_2q_4 + q_2q_3v_g^{\frac{1}{3}}\exp(3.5\ln^2\sigma_g) \tag{28}$$

$$v_{e2} = q_1q_4v_g^{-\frac{2}{3}}\exp(-10\ln^2\sigma_g) + q_1q_3v_g^{-\frac{1}{3}}\exp(-5.5\ln^2\sigma_g) + q_2q_4 + q_2q_3v_g^{\frac{1}{3}}\exp(6.5\ln^2\sigma_g) \tag{29}$$

The associated initial conditions of equations (24) - (26) are:

$$\text{at } x = 0,\ M_0 = N_i,\ M_1 = N_iv_{gi}\exp(4.5\ln^2\sigma_{gi}),\ M_2 = N_iv_{gi}^2\exp(18\ln^2\sigma_{gi}) \tag{30}$$

where subscript "i" represents the inlet condition.

Equations (24) - (26), along with the initial conditions, constitute a set of coupled ordinary differential equations (ODEs) that describe the continuous evolution of the first three moments of the distribution along the ESP. These ODEs are then solved by an IMSL stiff ODE solver, DIVPAG.[13]

Once the first three moments of the distribution are solved, the number efficiency of an ESP can be obtained from the evolution of M_0 while the mass efficiency of an ESP can be obtained from the evolution of M_1. The values of V_{e0} and V_{e1} are related to the number and mass average effective migration velocities, respectively. It must be noted that particles of different sizes are being collected by the ESP at different rates. This produces continuous changes in N, v_g, and σ_g, and thus results in variations of V_{e0}, V_{e1}, and V_{e2} along the ESP.

If other mechanisms are considered, they can be incorporated into equations (24) - (26). However, if only particle polydispersity is of concern, the calculation procedure can be simplified by assuming no variations of V_{e0}, V_{e1}, and V_{e2} over a spatial step size (Δx). Therefore equations (24) - (26) are integrated to obtain a form similar to the Deutsch-Anderson equation, given by

$$M_0^m = M_{0i}\exp\left(-\frac{2x^m}{wU_{av}}V_{e0}^m\right) \tag{31}$$

$$M_1^m = M_{1i}\exp\left(-\frac{2x^m}{wU_{av}}V_{e1}^m\right) \tag{32}$$

$$M_2^m = M_{2i}\exp\left(-\frac{2x^m}{wU_{av}}V_{e2}^m\right) \tag{33}$$

where superscript "m" denotes the calculation steps, and x^m is equal to $m\bullet\Delta x$.

The computation effort required using equations (31) - (33) is much simpler than that using equations (24) - (26). It can be done on a calculator or using spreadsheet software. By starting with the inlet v_g and σ_g, the inlet values of V_{e0}, V_{e1}, and V_{e2} are obtained from equations (27) -(29). And using the values of V_{e0}, V_{e1}, V_{e2}, and equation (30), the first three moment equations (31) - (33) are solved to obtain the new values of v_g and σ_g at the next spatial step. The procedure is repeated step-by-step to determine the first three moments of the distribution at any location in an ESP.

Space Charge Effect

Derivation of the above equations was based on ignoring the space charge effect. The space charge effect, which enhances the electric field strength, may be important if the inlet particle number concentration is high. The electric field strength at the collector surface for a plate-plate ESP which considers the space charge can be derived from the Gauss law[14]

$$E_c = \frac{q_v w}{4\varepsilon_0} + E_{av} \tag{34}$$

where q_v is the space charge density (= q N). Therefore as particles are continuously collected, the values of q_v and E_c vary along the ESP.

When equations (12), (15), and (34) are substituted into equation (7), the effective migration velocity of a particle, considering the space charge effect, is written as

$$V_e=(q_1^2 q_4 v^{-\frac{2}{3}}+q_1^2 q_3 v^{-\frac{1}{3}}+2q_1 q_2 q_4+2q_1 q_2 q_3 v^{\frac{1}{3}}+q_2^2 q_4 v^{\frac{2}{3}}+q_2^2 q_3 v)N + (q_1 q_6 v^{-\frac{2}{3}}+q_1 q_5 v^{-\frac{1}{3}}+q_2 q_6+q_2 q_5 v^{\frac{1}{3}}) \tag{35}$$

where

$$q_5 = \frac{wC^*}{12\pi\mu\epsilon_0}\left(\frac{\pi}{6}\right) \tag{36}$$

and

$$q_6 = \frac{3.314\lambda w}{12\pi\mu\epsilon_0}\left(\frac{\pi}{6}\right)^{\frac{2}{3}} \tag{37}$$

By substituting equation (35) into equation (6), multiplying both sides by v_i dv, and integrating over the entire particle size range, equations (24) - (26) are also derived. The only difference between considering and neglecting the space charge effect is in the formulations of the three particle migration velocities, given by

$$V_{e0}=[q_1^2 q_6 v_g^{-\frac{2}{3}}\exp(2\ln^2\sigma_g)+q_1^2 q_5 v_g^{-\frac{1}{3}}\exp^{\frac{1}{3}}(0.5^2\ln^2\sigma_g)+2q_1 q_2 q_6 + 2q_1 q_2 q_5 v_g^{\frac{1}{3}}\exp(0.5\ln^2\sigma_g)+q_2^2 q_6 v_g^{\frac{2}{3}}\exp(2\ln^2\sigma_g)+q_2^2 q_5 v_g\exp(4.5\ln^2\sigma_g)]M_0 + q_1 q_4 v_g^{-\frac{2}{3}}\exp(2\ln^2\sigma_g)+q_1 q_3 v_g^{-\frac{1}{3}}\exp(0.5\ln^2\sigma_g)+q_2 q_4+q_2 q_3 v_g^{\frac{1}{3}}\exp(0.5\ln^2\sigma_g) \tag{38}$$

$$V_{e1}=[q_1^2 q_6 v_g^{-\frac{2}{3}}\exp(-4\ln^2\sigma_g)+q_1^2 q_5 v_g^{-\frac{1}{3}}\exp(-2.5\ln^2\sigma_g)+2q_1 q_2 q_6 + 2q_1 q_2 q_5 v_g^{\frac{1}{3}}\exp(3.5\ln^2\sigma_g)+q_2^2 q_4 v_g^{\frac{2}{3}}\exp(8\ln^2\sigma_g)+q_2^2 q_5 v_g\exp(13.5\ln^2\sigma_g)]M_0 + q_1 q_4 v_g^{-\frac{2}{3}}\exp(-4\ln^2\sigma_g)+q_1 q_3 v_g^{-\frac{1}{3}}\exp(-2.5\ln^2\sigma_g)+q_2 q_4+q_2 q_3 v_g^{\frac{1}{3}}\exp(3.5\ln^2\sigma_g) \tag{39}$$

$$V_{e2}=[q_1^2 q_6 v_g^{-\frac{2}{3}}\exp(-10\ln^2\sigma_g)+q_1^2 q_5 v_g^{-\frac{1}{3}}\exp(-5.5\ln^2\sigma_g)+2q_1 q_2 q_6 + 2q_1 q_2 q_5 v_g^{\frac{1}{3}}\exp(6.5\ln^2\sigma_g)+q_2^2 q_4 v_g^{\frac{2}{3}}\exp(14\ln^2\sigma_g)+q_2^2 q_5 v_g\exp(22.5\ln^2\sigma_g)]M_0 + q_1 q_4 v_g^{-\frac{2}{3}}\exp(-10\ln^2\sigma_g)+q_1 q_3 v_g^{-\frac{1}{3}}\exp(-5.5\ln^2\sigma_g)+q_2 q_4+q_2 q_3 v_g^{\frac{1}{3}}\exp(6.5\ln^2\sigma_g) \tag{40}$$

RESULTS AND DISCUSSION

Model Verification

Except for the purpose of comparison with experimental data available in the literature, predictions were made based on the parameter values listed in Table 1. The stability of numerical solutions predicted by equations (24) - (26) and (31) - (33) as a function of spatial step sizes (Δx) was first investigated by comparing the overall mass efficiency of an ESP. Trails with varying Δx from 0.1 to 10^{-6} m, which correspond to ΔSCA of 0.5 to 5 x 10^{-6} s m^{-1}, were conducted and the results were that nearly identical solutions were observed for $\Delta x \leq 0.01$ m. Therefore Δx of 0.01 m was used in the following predictions.

The overall mass efficiency of an ESP predicted by the present model was then compared with the efficiency predicted by Feldman's model.[3] Figure 3 shows the comparison results as a function of SCA. The inlet MMD and σ_g were selected as 2 μm and 2, respectively. The difference between the two models is that the present model predicted the overall mass efficiency in terms of the evolution of the first volume moment (M_1), while the Feldman's model calculated the grade efficiency of each particle size and then integrated it over all particle size regimes. Figure 3 shows that a reasonable agreement was obtained between the two models.

The differences in predicting the overall mass efficiency using Cochet's equation and the modified form of Cochet's

Table 1. Parameters used in the study of an ESP performance.

Parameters	Values	Unit
mass loading	5	g m^{-3}
particle density	2270	kg m^{-3}
E_{av}	5	kV cm^{-1}
U_{av}	1	m s^{-1}
w	0.4	m
μ	2.4x10^{-5}	kg m^{-1}
ε_0	8.85x10^{-12}	F m^{-1}
λ	0.065	μm
λ_i	0.1	μm
κ	5	

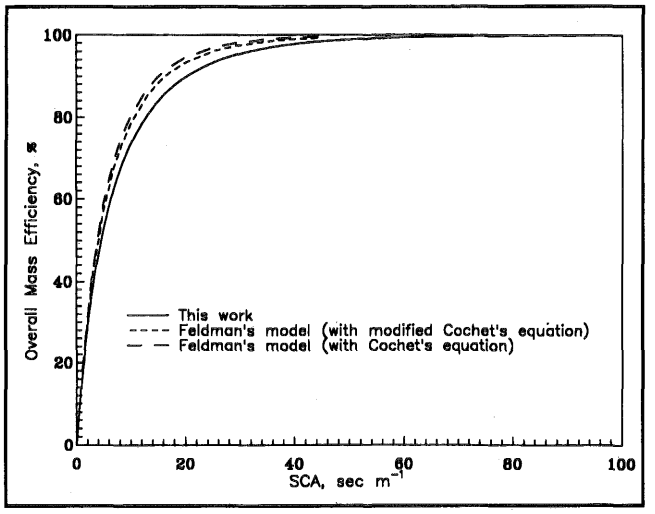

Figure 3. The overall mass efficiencies predicted by the present model and by the Feldman's model using the modified Cochet's equation and Cochet's equation.

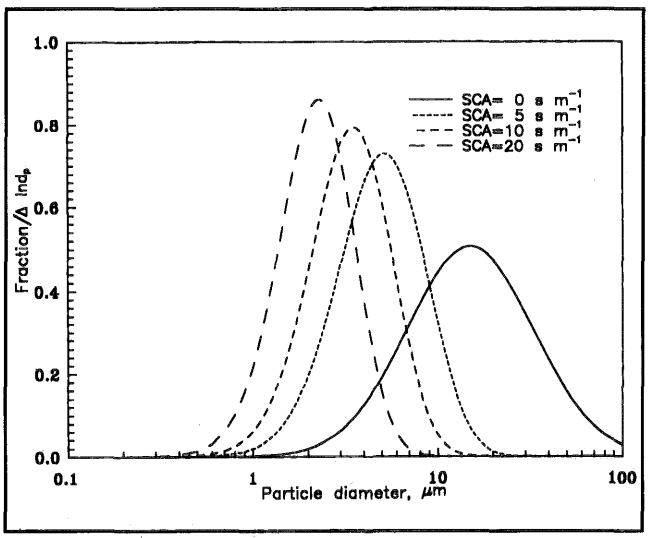

Figure 4. The evolution of the particle size distribution obtained by computing the grade efficiency of each size. The inlet particle MMD and σ_g were 15 μm and 2.2.

equation were evaluated and the results are also shown in Figure 3. Since Cochet's equation is not an integrable form, it can not be used in the present model. Therefore a comparison of the two charge equations was made using Feldman's model. As Figure 3 shows, these two charge equations yield close results in the overall mass efficiency. The maximum deviations between these two charge equations are less than 1% for the overall mass efficiency, and about 10% for the grade efficiency as the value of $2\lambda_i/d_p$ equals 1.

The lognormal conservation of the particle size distribution in an ESP was then investigated. Figure 4 shows the evolution of the particle size distribution along an ESP. The inlet particle MMD and σ_g are 15 μm and 2.2, respectively. As can be seen, when starting with a lognormal inlet particle size distribution (SCA = 0), the distribution shifts continuously to the finer particles as SCA becomes larger. But the size distribution can still be approximated well by a

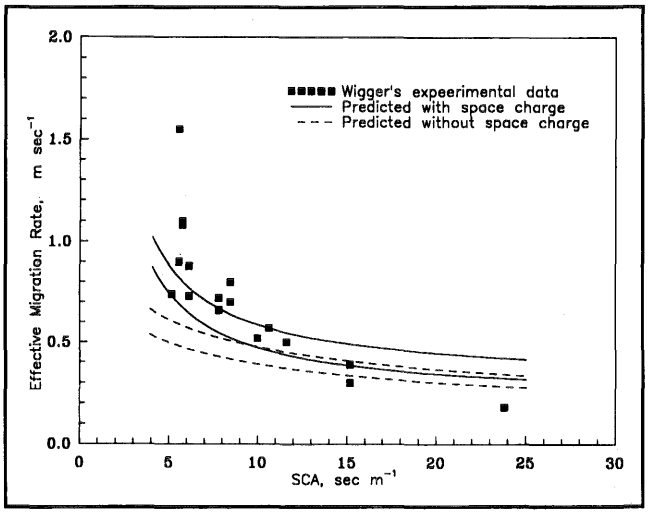

Figure 5. Comparison of the effective migration velocities predicted by the present model with the experimental data documented by Wiggers.[15]

lognormal function. This is observed from the Gaussian shape of the distribution when it is plotted on a logarithmic scale, and may be attributed to the fact that both very large and very fine particles are collected efficiently by field charging and diffusion charging, respectively. As a result, the particle size distribution remains a lognormal function along an ESP, without a significant deviation.

Space Charge Effect

Figure 5 shows a comparison of the effective migration velocities predicted by the present model with the experimental data documented by Wiggers.[15] His experimental conditions are summarized as: the ESP was 3 meters in length and the average electric field strength was 6.4 ± 0.6 kV cm^{-1}. The variation in SCA was controlled by variable plate spacing. A quartz dust with inlet MMD and σ_g of around 8.5 μm and 2.5 was employed. The dielectric constant was assumed to be 10 for the quartz dust. Predictions were made both considering and neglecting the space charge effect. As can be seen in Figure 5 for small SCAs, the model predictions which considered the space charge effect resulted in better agreement than those that neglected the space charge effect. On the other hand, for large SCAs the space charge effect is not significant, and both compare well with Wiggers' experimental data.

Figure 6 shows the overall mass efficiency as a function of inlet particle MMD when the space charge effect is considered and when it is neglected. The SCA was 40 s m^{-1} and the inlet σ_g was 2. As can be seen, the space charge effect was significant for inlet particle MMDs in the range of around 0.03 to 1 μm. However, for the typical range of particle MMDs (2 - 20 μm) encountered in many industrial combustion processes,[16] the space charge effect may be neglected.

Particle Size Distribution Effect

Evolution of the size distribution. Figures 7a and 7b show the evolutions of σ_g and MMD as a function of SCA for inlet

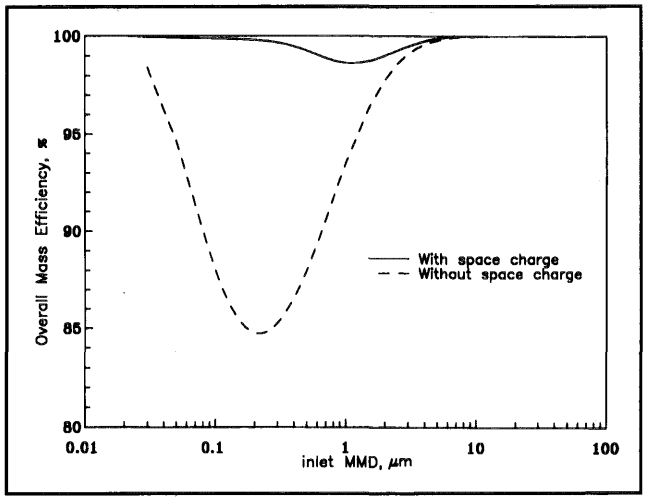

Figure 6. The predicted overall mass efficiencies as a function of inlet particle MMD with considering and neglecting the space charge effect. The SCA was 40 s m^{-1} and the inlet σ_g was 2.

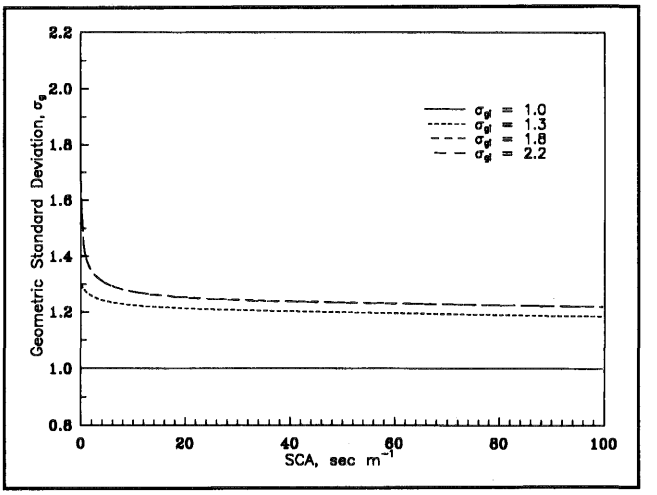

Figure 7a. The evolution of σ_g as a function of SCA for inlet particle MMD of 2 μm with different σ_gs.

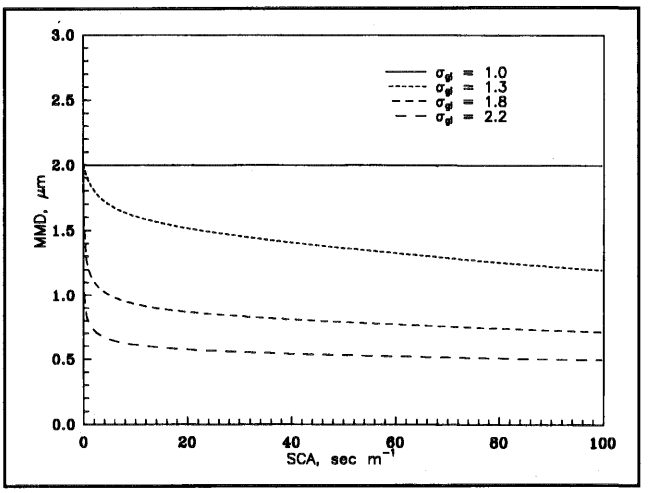

Figure 7b. The evolution of particle MMD as a function of SCA for inlet particle MMD of 2 μm with different σ_gs.

particles with different σ_gs. The inlet particle was 2 μm and the space charge effect was considered. As can be seen, both σ_g and MMD drop quickly as particles enter an ESP, and then the rates of change for σ_g and MMD slow down. This is because both very large and very fine particles are captured almost immediately after entering an ESP. The remaining particles whose sizes fall in the range of around 0.1 - 1 μm require more time to be captured.

Overall mass efficiency. The overall mass efficiencies as a function of inlet particle MMD with different s_gs are shown in Figure 8a. The SCA was 10 s m^{-1} and the space charge effect was considered. If the inlet particle MMD is large (e.g., 15μm), the ESP tends to have a higher overall mass efficiency for inlet particles with a narrow spread (e.g. s_g = 1.0) than for those with a wide spread (e.g., s_g = 2.2). This is because inlet particles with a large MMD but a narrow spread (which includes most particles in the dust stream) are very large and can be collected efficiently. On the other hand, the trend is opposite for a small inlet particle MMD (e.g., 1 μm). However, as will be shown later in Figure 8c, this observation is valid only for a small SCA or at the early stage of an ESP.

Figure 8b shows the overall mass efficiencies as a function of SCA for inlet particles with different σ_gs. The inlet particle MMD was 15 μm. As the figure shows, the overall mass efficiency decreases with increasing particle polydispersity at all SCAs.

Figure 8c shows the overall mass efficiencies as a function of SCA for inlet particles with different σ_gs. The inlet particle MMD was 1 μm. At SCAs less than 30 s m^{-1}, the overall mass efficiency increases with increasing particle polydispersity. However, the opposite trend is observed at SCAs larger than 34 s m^{-1}. This is because inlet particles with a wide spread (e.g., σ_g = 2.2) tend to lose coarse particles to the collector surface at a fast rate, which may lead to a high overall mass efficiency at the early stage of an ESP. But as the SCA increases, the uncollected particles are in the size range of charging difficulty (0.2 - 2 μm). Therefore, the particle collection rate slows down, and the overall mass efficiency may become lower than for those with a narrow spread. And as Figures 8b and 8c show, it is expected that inlet particles with a narrow spread eventually have a high overall mass efficiency at large SCAs, no matter whether the inlet particle MMD is large or small.

Overall number efficiency. Figure 9a shows the overall number efficiencies as a function of inlet particle MMD with different s_gs. The SCA was 10 s m^{-1} and the space charge effect was considered. It is seen that variations of the overall number efficiency with respect to particle polydispersity are similar to those shown in Figure 8a for very large and very small inlet particle MMDs. On the other hand, for particles whose inlet MMD is in the range of charging difficulty (0.2 - 2 μm), variations of the overall number efficiency with respect to particle polydispersity are quite different from those of the overall mass efficiency. For example, for inlet particles with an s_g of 2.2 the minimum overall mass and number efficiencies occur at the same inlet MMD of around

2 μm. But the minimum overall mass efficiency (~90%) is higher than that of monodisperse particles (~82%) while the minimum overall number efficiency (~70%) is lower than that of monodisperse particles (~82%).

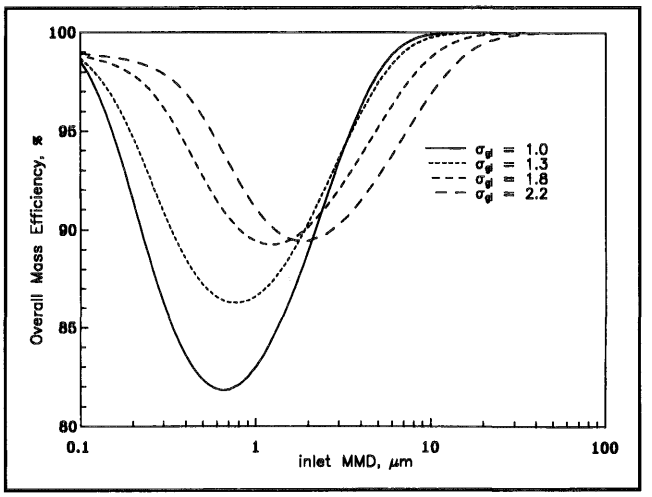

Figure 8a. The predicted overall mass efficiencies as a function of inlet particle MMD for different σ_gs. The SCA was 10 s m^{-1}.

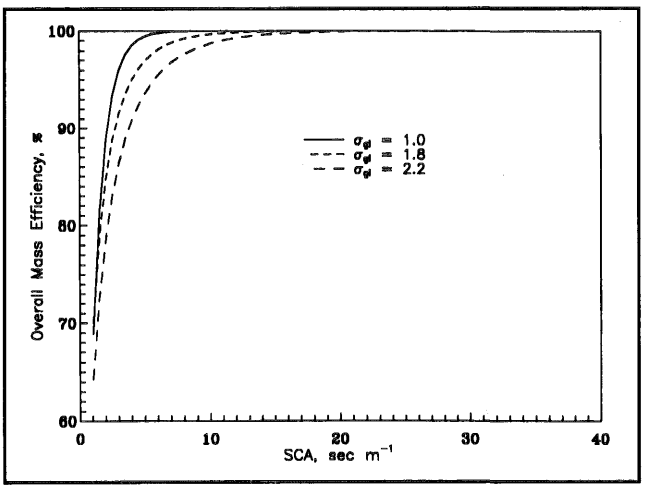

Figure 8b. The predicted overall mass efficiencies as a function of SCA for inlet particles with different σ_gs. The inlet particle MMD was 15 μm.

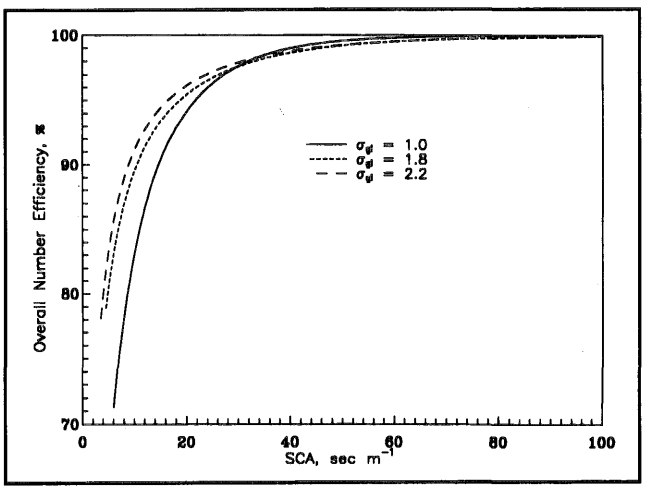

Figure 8c. The predicted overall mass efficiencies as a function of SCA for inlet particles with different σ_gs. The inlet particle MMD was 1 μm.

Figures 9b and 9c show the overall number efficiencies as a function of SCA for inlet particle MMDs of 15 μm and 1 μm, respectively. As can be seen in Figure 9b, the overall number efficiency decreases with increasing particle

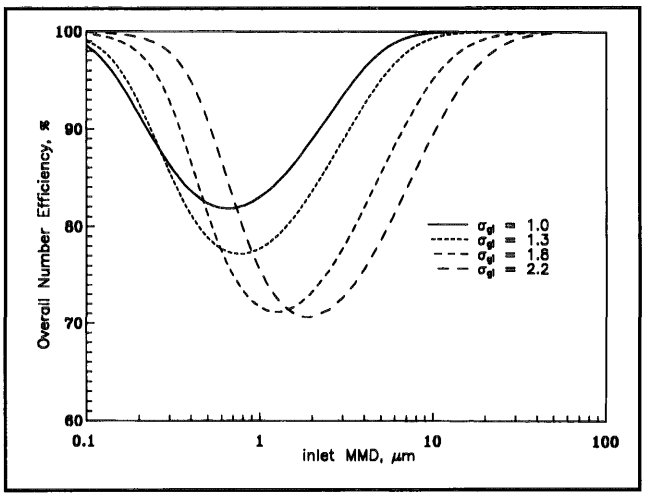

Figure 9a. The predicted overall number efficiencies as a function of inlet particle MMD with different σ_gs. The SCA was 10 s m^{-1}.

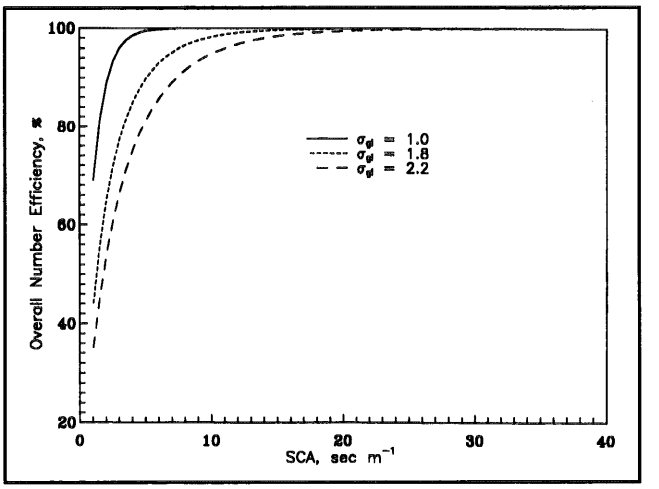

Figure 9b. The predicted overall number efficiencies as a function of SCA for inlet particles with different σ_gs. The inlet particle MMD was 15 μm.

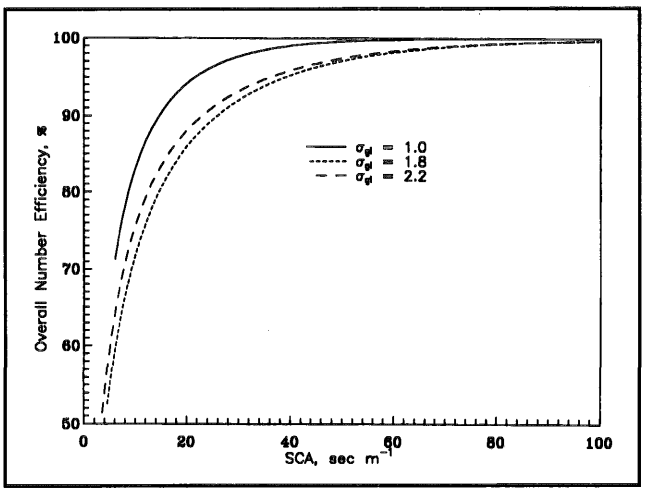

Figure 9c. The predicted overall number efficiencies as a function of SCA for inlet particles with different σ_gs. The inlet particle MMD was 1 μm.

polydispersity for inlet particle MMD of 15 μm at all SCAs. This observation is similar to variations of the overall mass efficiency shown in Figure 8b. On the other hand, as indicated in Figure 9c for inlet particle MMD of 1 μm, there is no clear trend for variations of the overall number efficiency with respect to the particle polydispersity.

CONCLUSIONS

This study demonstrated the use of moments in terms of a lognormal size distribution function to predict the overall mass and number efficiencies of an ESP. Two sets of equations which result in analogous solutions were presented. The first set of equations (equations [24] -[26]) must be done using numerical analysis, while the second set of equations (equations [31] - [33]) can easily be done even with a calculator. Equations (31) - (33) are practical for a primary design of an ESP while equations (24) - (26) can be employed and extended if more complicated mechanisms are to be incorporated into the model. Both formulations of the effective migration velocities of considering and neglecting the space charge effect were also presented.

The performance of the present model was validated by comparing its predicted overall mass efficiencies as well as effective migration velocities with previous studies in the literature. The effects of the particle size distribution of MMD and σ_g on the overall mass and number efficiencies were then investigated and quantitatively determined.

The advantages of the present model lie in the fact that it predicts the overall mass and number efficiencies of polydisperse particles without having to compute the grade efficiency of each particle size. In addition, the total particle surface available (represented by $M_{2/3}$) for deposition of heavy metal vapors as well as the stack opacity (represented by M_2) which leads to the visibility problem can also be readily calculated using the present model.

ACKNOWLEDGMENTS

Support from the National Science Council, Republic of China, through grant number NSC 84-2211-E-009-002 is gratefully acknowledged.

NOMENCLATURE

A_c = Collector surface area
A_p = Cross sectional area of ESP
C = Cunningham slip correction factor
d_p = Particle diameter
E_{av} = Average electric field strength
E_c = Electric field strength at the collector surface
E_∞ = Local electric field strength
h = Height of collecting plate
M_j = jth moment of particle size distribution
MMD = Mass median diameter
n = Particle size distribution function
N = Particle number concentration
Q = Volumetric flow rate of gas through the unit
q = Particle charge
q_v = Space charge density
SCA = Specific collecting area
U_{av} = Average dust flow velocity through the unit
V_e = Effective migration velocity of particles
v = Particle volume
v_g = Geometric average particle volume
x = Axial distance
w = Space between two parallel plates

Greek Symbols

η = Collection efficiency
κ = Dielectric constant of particles
μ = Flow viscosity
λ = Mean free path of the gas
λ_i = Mean free path of the ion
ε_o = Permittivity of free space
σ_g = Geometric standard deviation

Subscript

$_i$ = Inlet condition

REFERENCES

1. White, H.J. *Industrial Electrostatic Precipitator;* Addison-Wesley: Reading, MA, 1963.
2. Benìtez, J. *Process Engineering and Design for Air Pollution Control;* PTR Prentice Hall: Rahway, NJ, 1993.
3. Feldman, P.L. "Effects of particle size distribution on the performance of electrostatic precipitators," Paper No. 75-02-3, in *Proceedings of 68th Air Pollution Control Association Conference;* Air Pollution Control Association: Pittsburgh, PA, 1975.
4. Gooch, J.P.; Francis, N.L. "A theoretically based mathematical model for calculation of electrostatic precipitator performance," *J. Air Poll. Cont. Assoc.* **1975**, *25*, 108-113.
5. Riehle, C.; Löffler, F. "The effective migration rate in electrostatic precipitators," *Aerosol Sci. Technol.* **1992**, *16*, 1-14.
6. Matts, S.; Ohnfeldt, P. "Efficient gas cleaning with SF electrostatic precipitator," Flakt, 1-12. Cited in Lawless, P.A.; Sparks, L.E. "A review of mathematical models for ESPs and comparison of their successes," in *Proceedings of Second International Conference on Electrostatic Precipitation,* Kyoto, Japan, 1984, 513-522.
7. Davison, R.L.; Natusch, D.F.S.; Wallace, J.R.; Evans, Jr., C.A. "Trace elements in fly ash - dependence of concentration on particle size," *Environ. Sci. Technol.* **1974**, *8*, 1107.
8. Flagan, R.C.; Seinfeld, J.H. *Fundamentals of Air Pollution Engineering;* Prentice Hall: Rahway, NJ, 1988.
9. Licht, W. *Air Pollution Control Engineering,* Marcel Dekker: New York, NY 1988.
10. Bai, H.; Biswas, P. "Deposition of lognormally distributed aerosols accounting for simultaneous diffusion, thermophoresis and coagulation," *J. Aerosol Sci.* **1990**, *21*, 629-640.
11. Friedlander, S.K. *Smoke, Dust and Haze;* John Wiley & Sons: New York, NY, 1977.
12. Lee, K.W.; Chen, H.; Gieseke, J.A."Log-normally preserving size distribution for Brownian coagulation in the free molecule regime," *Aerosol Sci. Technol.* **1984**, *3*, 53-62.
13. IMSL Contents Document. International Mathematics And Statistics Libraries, Houston 2, Version 1.0, 1987.
14. Crawford, M. *Air Pollution Control Theory;* McGraw-Hill: New York, NY, 1976.
15. Wiggers, H. Dissertation. Universität Essen. Fortschr. Ber. VDI-Z. Reihe 3, Nr. 67, 1982. Cited in Reference 5.
16. Buonicore, A.J.; Davis, W.T. *Air Pollution Engineering Manual;* Van Nostrand Reinhold: New York, NY, 1992

About the Authors

H. Bai, Ph.D. (corresponding author) is an associate professor in the Institute of Environmental Engineering, National Chiao-Tung University, 75, Po-Ai St., Hsin-Chu, Taiwan. C. Lu, Ph.D. is an associate professor in the Department of Environmental Engineering, National Chung Hsing University, Taichung, Taiwan. C.L. Chang is currently a graduate student working on his doctorate degree in the Institute of Environmental Engineering, National Chiao-Tung University, Taiwan.